Microbial metabolism and adaptations in *Atribacteria*-dominated methane hydrate sediments

Jennifer B. Glass[1*], Piyush Ranjan[2#], Cecilia B. Kretz[§], Brook L. Nunn[3], Abigail M. Johnson[1], Manlin Xu[1], James McManus[4], Frank J. Stewart[2,5]

[1]School of Earth and Atmospheric Sciences, Georgia Institute of Technology, Atlanta, GA, USA; [2]School of Biological Sciences, Georgia Institute of Technology, Atlanta, GA, USA; [3]Department of Genome Sciences, University of Washington, Seattle, WA; [4]Bigelow Laboratory for Ocean Sciences, East Boothbay, ME, USA; [5]Department of Microbiology & Immunology, Montana State University, Bozeman, MT, USA

*Corresponding Author: jennifer.glass@eas.gatech.edu

[#]Now at: Michigan Medicine, University of Michigan, Ann Arbor, Michigan, USA;

[§]Now at: Association of Public Health Laboratories, Manager of Emerging and Zoonotic Infectious Diseases, Silver Spring, MD, USA

Running Title: *Atribacteria* adaptions in methane hydrate ecosystem

Dedication: To Katrina Edwards

Originality-Significance Statement: This work provides insights into the metabolism and adaptations of microbes that are ubiquitous and abundant in methane-rich ecosystems. Our findings suggest that bacterial fermentation is a source of acetate for aceticlastic methanogenesis and a driver of iron reduction in the metal reduction zone. *Atribacteria*, the most abundant phylum in gas hydrate-bearing sediments, possess multiple strategies to cope with environmental stress.

Summary: Gas hydrates harbor gigatons of natural gas, yet their microbiomes remain understudied. We bioprospected 16S rRNA amplicons, metagenomes, and metaproteomes from methane hydrate-bearing sediments under Hydrate Ridge (offshore Oregon, USA, ODP Site 1244, 2-69 mbsf) for novel microbial metabolic and biosynthetic potential. *Atribacteria* sequences generally increased in relative sequence abundance with increasing sediment depth. Most Atribacteria ASVs belonged to JS-1-Genus 1 and clustered with other sequences from gas hydrate-bearing sediments. We recovered 21 metagenome-assembled genomic bins spanning three geochemical zones in the sediment core: the sulfate-methane transition zone, metal (iron/manganese) reduction zone, and gas hydrate stability zone. We found evidence for bacterial fermentation as a source of acetate for aceticlastic methanogenesis and as a driver of iron reduction in the metal reduction zone. In multiple zones, we identified a Ni-Fe hydrogenase-Na+/H+ antiporter supercomplex (Hun) in *Atribacteria* and *Firmicutes* bins and in other deep subsurface bacteria and cultured hyperthermophiles from the *Thermotogae* phylum. *Atribacteria* expressed tripartite ATP-independent (TRAP) transporters downstream from a novel regulator (AtiR). Atribacteria also possessed adaptations to survive extreme conditions (e.g., high salt brines, high pressure, and cold temperatures) including the ability to synthesize the osmolyte di-myo-inositol-phosphate as well as expression of K^+-stimulated pyrophosphatase and capsule proteins.

Introduction

Gas clathrate hydrates are composed of solid water cages encasing gas molecules, commonly methane (CH_4). Methane hydrates form naturally under high pressure and low temperature along continental margins (Kvenvolden, 1993; Mazurenko and Soloviev, 2003; Hester and Brewer, 2009; Collett et al., 2015). Continental margins and shelves harbor gigatons of natural gas in hydrates, which are susceptible to dissociation due to rising ocean temperatures, with potential for releasing massive methane reservoirs to the ocean and the atmosphere, which could exacerbate global warming (Archer et al., 2009; Ruppel and Kessler, 2017).

Despite the global importance of gas hydrates, their microbiomes remain largely unknown. Microbial cells are physically associated with hydrates (Lanoil et al., 2001), and the taxonomy of these hydrate-associated microbiomes is distinct from non-hydrate-bearing sites (Inagaki et al., 2006), possibly due to more extreme environmental conditions. Because salt ions are excluded during hydrate formation, porewaters of hydrate-bearing sediments are hypersaline (Ussler III and Paull, 2001; Bohrmann and Torres, 2006). Hydrate-associated microbes may possess adaptations to survive high salinity and low water activity, as well as low temperatures and high pressures (Honkalas et al., 2016). However, knowledge of the genetic basis of such adaptations is incomplete, as genomic data for hydrate communities are sparse and most hydrate microbiomes have been characterized primarily through single-gene taxonomic surveys.

Global 16S rRNA gene surveys show that the JS-1 sub-clade of the uncultivated bacterial candidate phylum *Atribacteria*, also known as *Caldiatribacteriota*, is the dominant taxon in gas hydrates (Reed et al., 2002; Inagaki et al., 2003; Kormas et al., 2003; Newberry et al., 2004; Webster et al., 2004; Inagaki et al., 2006; Webster et al., 2007; Fry et al., 2008; Kadnikov et al., 2012; Parkes et al., 2014; Yanagawa et al., 2014; Chernitsyna et al., 2016; Gründger et al., 2019) and in other marine and freshwater sediment ecosystems with abundant methane (Blazejak and Schippers, 2010; Gies et al., 2014; Carr et al., 2015; Hu et al., 2016; Nobu et al., 2016; Lee et al., 2018; Bird et al., 2019). The other major *Atribacteria* lineage, OP-9, primarily occurs in hot springs (Dodsworth et al., 2013; Rinke et al., 2013) and thermal bioreactors (Nobu et al., 2015). Marine *Atribacteria* are dispersed through ejection from submarine mud volcanoes (Hoshino et al., 2017; Ruff et al., 2019), and environmental heterogeneity may select for locally adapted genotypes. *Atribacteria* are highly enriched in anoxic, organic, and hydrocarbon rich sediments (Chakraborty et al., 2020; Hoshino et al., 2020) and have recently been discovered to be actively reproducing in the deep subsurface (Vuillemin et al., 2020). The phylogenetic diversity of *Atribacteria* genera suggests the potential for uncharacterized variation in functional niches.

Atribacteria appear to rely primarily on heterotrophic fermentative metabolisms. The high-temperature OP-9 lineage ferments sugars to hydrogen, acetate, and ethanol (Dodsworth et al., 2013; Katayama et al., 2020). The low-temperature JS-1 lineage ferments propionate to hydrogen, acetate, and ethanol (Nobu et al., 2016). Some JS-1 strains can also ferment short-chain n-alkanes (e.g. propane) into fatty acids by fumarate addition (Liu et al., 2019). Both JS-1 and OP-9 lineages possess genes encoding bacterial microcompartment shell proteins that may sequester toxic aldehydes and enable their condensation to carbohydrates (Nobu et al., 2016). Marine sediment JS-1 express genes to use allantoin as an energy source or chemical protectant and, unlike most deep subsurface bacteria, also encode a membrane-bound hydrogenase complex cotranscribed with an oxidoreductase, suggesting the ability for anaerobic respiration (Bird et al., 2019).

Here we examined the distribution, phylogeny, and metabolic potential of uncultivated JS-1 *Atribacteria* beneath Hydrate Ridge, off the coast of Oregon, USA, using a combination of 16S rRNA gene amplicon, metagenomic, and metaproteomic analysis. We found that *Atribacteria* from JS-1 Genus-1 are abundant throughout in the gas hydrate stability zone (GHSZ) and that they harbor numerous strategies for tolerance of osmotic stress, including many biosynthesis pathways for unusual osmolytes.

Results and Discussion

Geochemical gradients. Sediment core samples spanned three geochemical zones from 0-69 meters below seafloor (mbsf) at the ODP Site 1244 at Hydrate Ridge, off the coast of Oregon, USA (Fig. S1; Tréhu et al., 2003): the sulfate-methane transition zone (SMTZ; 2-9 mbsf; cores C1H2, C1H3, F2H4), the metal (iron/manganese) reduction zone (MRZ; 18-36 mbsf; cores F3H4, C3H4, E5H5), and the GHSZ (45-124 mbsf; cores E10H5, E19H5; Fig. 1A, Table S1). Sediment porewater methane concentrations (approximate, due to loss during sampling) increased from negligible at the seafloor to 8% by volume at 3-5 mbsf, and remained <5% below 5 mbsf, except for sample C3H4 (21 mbsf, MRZ) with ~18% methane (Fig. 1A). Sulfate dropped from 28 to <1

mM from 0-9 mbsf (the SMTZ) and remained <1 mM below 9 mbsf (Fig. 1A). In the MRZ, dissolved Mn and Fe peaked at 6 and 33 μM, respectively, while outside of the MRZ, dissolved Mn was ~1 μM and dissolved Fe was 7-20 μM (Fig. 1A). Dithionite-extractable (see Roy et al. (2013)), termed here "reactive", Fe (0.4-1.4%) and Mn (0.002-0.012%) generally increased with depth (Table S1). Total organic carbon concentrations varied between 1-2 weight % (Table S1). Gas hydrate was observed from 45-125 mbsf in freshly recovered sediment cores, which contained up to 20% hydrate in the pore space, primarily as hydrate lenses or nodule patches (Tréhu et al., 2004; Fig. 1A). Estimated *in situ* salinity ranged from seawater salinity (35 g kg^{-1}) to >100 g kg^{-1} and was highest in the GHSZ (Milkov et al., 2004). *In situ* temperature ranged from ~4°C at the seafloor to ~6-11°C in the GHSZ (ShipboardScientificParty, 2003).

Atribacteria dominate ASVs in gas hydrate stability zone. *Actinobacteria, Atribacteria, Chloroflexi,* and *Planctomycetota* were the dominant bacterial phyla at Site 1244 (Fig. 1B). *Asgardarchaeota* and *Thermosplasmata* were the dominant archaeal phyla, with a notable rise in *Hadesarchaea* in the MRZ. Phylogenetic diversity in 16S rRNA gene amplicons based on the Shannon index and species richness based on the Chao1 index were highest in the SMTZ and MRZ, and lowest in the zones dominated by *Atribacteria*, in between the SMTZ and MRZ, and in the GHSZ (Fig. 1C). The relative sequence abundance of *Atribacteria* 16S rRNA amplicons ranged from 10-15% in the near surface to 80-85% at the top of the MRZ and the GHSZ (Fig. 1B). Most of the *Atribacteria* ASVs (n=20) belonged to JS-1 Genus 1 and clustered with other seep- and hydrate-associated sequences (Fig. 2A). ASV_368 comprised 54% of all amplicons in the GHSZ, and most GenBank sequences with 100% similarity to ASV_368 were from hydrate-bearing sediments from the Pacific Ocean basin (Table S2).

Metagenome-assembled binning yielded 21 MAGs with >35% completeness and <10% contamination including 17 bacteria and 4 archaea (Table S3). These MAGs included five *Dehalococcoidia* (*Chloroflexi*) in the SMTZ, MRZ, and GHSZ, and five *Firmicutes* (*Clostridia*) in

127 the SMTZ and MRZ (Table S3). Other MAGs included one *Calditrichaeota* in the SMTZ, one each
128 of *Bacteroidetes*, *Spirochaeta, Hadesarchaea*, and *Methanosarcinales* (*Euryarchaeota*) in the
129 MRZ, and one *Atribacteria* in the GHSZ (MAG E10H5-B2). The higher relative sequence
130 abundance of *Atribacteria* 16S rRNA sequences at the top of the MRZ and the GHSZ is consistent
131 with higher read recruitment (~4-8%) of *Atribacteria* MAG E10H5-B2 metagenomes from those
132 zones vs. other depths (<1%). Although E10H5-B2 lacked a 16S rRNA gene, the 16S rRNA gene
133 in RS-JS1 was 99.68% identical to 16S rRNA sequences from hydrate sediments from offshore
134 Japan (Shimokita Peninsula) and Taiwan (Lin et al., 2014), and 99.43% identical to a clone from
135 the South China Sea (Li and Wang, 2013; Fig. 2A, Table S2). Phylogeny based on eight
136 concatenated ribosomal proteins confirmed that MAG E10H5-B2 belonged to JS-1 Genus 1, and
137 formed a monophyletic group with MAGs from petroleum seeps in the Gulf of Mexico (E44-bin65;
138 Dong et al., 2019; Chakraborty et al., 2020) and marine sediments in the Ross Sea (RS-JS1; Lee et
139 al., 2018; Fig. 2B). Average amino acid identities between MAGs in JS-1 Genus 1 was 72-83%
140 (Table S4).

141 **Anaerobic hydrocarbon degradation, aceticlastic methanogenesis, and fermentative**
142 **iron reduction.** A recent study suggested that JS-1 can anaerobically degrade short-chain *n*-alkanes
143 using fumarate addition enzymes (FAEs; Liu et al., 2019). Like oil reservoir *Atribacteria*, MAG
144 E10H5-B2 contained genes encoding the glycyl radical protein subunit A (*faeA,* RXG63988, in the
145 pyruvate formate lyase family) and D (*faeD*, RXG63989) on the same contig. However, the *faeA*
146 gene product in MAG E10H5-B2 was shorter (786 aa) than in the oil reservoir MAGs (~860 aa)
147 and the *fae* operon lacked the signature *faeC* gene between *faeD* and *faeA* that is characteristic of
148 FAEs, suggesting that they may produce a different product.

149 Byproducts of fumarate addition enzymes (e.g., fatty acids) can be further degraded by
150 other bacterial fermentation in marine sediments. *Firmicutes* degrade benzoate to acetate and
151 transfer the electrons to crystalline Fe(III) minerals, producing dissolved Fe^{2+}; thereafter, the
152 acetate is converted to methane by syntrophic aceticlastic methanogenic archaea (Aromokeye et

153 al., 2020). The relative sequence abundance of *Firmicutes* and the presence of aceticlastic
154 *Methanosarcinales* (MAG F3H4-B6; Table S3) indicate that fermentative iron reduction was likely
155 the source of the Fe^{2+} peak and the methane peak in the MRZ **(Fig. 1A)**. Acetate for aceticlastic
156 methanogenesis could also come from other acetogens including *Atribacteria* (Carr et al., 2015).

157 A biogenic source of methane to the gas hydrates at Hydrate Ridge is consistent with
158 previous isotopic analyses (Kastner et al., 1998). Production of acetate by fermentative bacteria
159 below the SMTZ challenges the previous paradigm that acetate was completely consumed in the
160 SMTZ and therefore that biogenic methane in gas hydrates originated solely from
161 hydrogenotrophic methanogenesis via CO_2 reduction (Whiticar et al., 1995). However, the carbon
162 isotopic composition of methane in the gas hydrate at Hydrate Ridge is more consistent with a CO_2
163 reduction pathway, and there may be additional deeper sources of hydrogenotrophic methane that
164 mask the contribution from aceticlastic methanogenesis.

165 **Predicted respiratory function of novel Hun supercomplex.** Two MAGs (*Atribacteria*
166 E10H5-B2 and *Firmicutes* E5H5-B3) contained genes for a putative operon encoding a 16-subunit
167 respiratory complex, hereafter designated Hun. The *hun* operon was also present in *Atribacteria*
168 MAGs and SAGs from Baltic Sea sediments (Bird et al., 2019), in diverse deep biosphere bacterial
169 MAGs (e.g. *Atribacteria, Omnitrophica, Elusimicrobia*, *Bacteriodetes* (Fig. 3A, Table S5)), and in
170 hyperthermophilic bacterial isolates from the genus *Kosmotoga* (*Thermotogae* phylum; Fig. 3A).
171 *Atribacteria hun* genes likely encode a complex of four protein modules that couple H^+ and Na^+
172 translocation to H_2 production (Fig. 3B) based on their similarity to characterized proteins (Schut
173 et al., 2016).

174 Additional analysis provided more insights into Hun function and phylogeny. The large
175 hydrogenase subunit HunG was classified as a [NiFe] Group 4g-hydrogenase according to the
176 Hydrogenase Database (Søndergaard et al., 2016). Group 4g-hydrogenases are biochemically
177 unclassified but predicted to be ferredoxin-coupled and may couple reduced ferredoxin oxidation
178 to proton reduction and H^+/Na^+ translocation (Greening et al., 2016). Based on the similarity of

179 HunAB to anaerobic sulfite reductase (Asr) subunits A and B, which transfer electrons from
180 ferredoxin to the active site in AsrC (missing in the *hun* operon), HunABC likely accept electrons
181 from ferredoxin and pass them through iron-sulfur clusters to $2H^+$ for reduction to H_2 at HunEFGP's
182 Ni-Fe active site, as suggested by the presence of two conserved CxxC motifs (L1 and L2) for Ni-
183 Fe cofactor binding in HunG (Fig. 4A). Further analysis revealed that conserved residues for the
184 Ni-Fe active site were different for HunG than other hydrogenases: CGIC-CYCC vs. CGIC-CxxC
185 in other Group 4 hydrogenases (Fig. 4A). HunG was evolutionarily distant from other Group 4g
186 sequences (Fig. 4A, B). In some MAGs, a 4Fe-4S molybdopterin domain-containing protein was
187 present in between HunB and HunC (Fig. 3A). P-module-like subunits HunDHILK are predicted
188 to be proton-pumping transmembrane proteins and Na-module-like subunits HunIJKLMNO are
189 homologs of the Na^+/H^+ antiporter MnhABCDEFGH in Mrp-Mbh-type complexes. ATP is then
190 generated via Na^+-specific ATP synthases (Bird et al., 2019). Electrons from H_2 could be transferred
191 back to ferredoxin by the activity of the heterodisulfide reductase (HdrA)-methyl viologen
192 hydrogenase (MvhAGD) complex.

193 **Transporters expressed in metaproteome.** To assess gene expression, we analyzed
194 metaproteomes from a subset of Site 1244 cores (C1H2, C3H4, and E10H5, from ~2, 20, and ~69
195 mbsf, respectively). Although we recovered few peptides of high quality, several robust hits were
196 identified, including several types of transporters and cell envelope-associated proteins (Table 1).
197 The expressed proteins were identified using *Atribacteria* MAGs from IODP Site 1244 as the
198 reference database (see Methods) and had closest matches to other *Atribacteria* genomes (Table 1),
199 suggesting that they originated from *Atribacteria*. Expressed proteins included a high-affinity
200 branched-chain amino acid transport system permease (LivH) and multiple tripartite ATP-
201 independent (TRAP) transporters (Fig. 5A). TRAP transporters use an electrochemical gradient
202 (H^+ or Na^+) and a substrate-binding protein to transport a wide variety of molecules across the
203 membrane (Rosa et al., 2018). Conserved residues within the TRAP substrate-binding protein
204 confer specificity, with a conserved arginine residue essential for carboxylate transport (Fischer et

205 al., 2015). In JS-1 MAGs from oil reservoirs, TRAP transport genes were associated with fumarate
206 addition genes and likely transport fumarate or succinate for addition to hydrocarbons (Liu et al.,
207 2019). In MAG E10H5-B2, genes for choline, inositol, and D-galacturonate catabolism often
208 surrounded TRAP transporters (Fig. 5A), consistent with the finding that TRAP transporters can
209 transport a much broader range of compounds than originally known (Vetting et al., 2015).

210 **AtiR, a novel regulator**. Several of the expressed transporter proteins were encoded by
211 genes downstream from a novel gene predicted to encode an ~85-amino acid helix-turn-helix
212 xenobiotic response element (XRE) transcriptional regulator, which we named "AtiR" (Table S6;
213 Fig. 5). AtiR was present in other genomes from Site 1244, in an *Atribacteria* MAG from marine
214 hydrothermal sediment from Guaymas Basin (Zhou et al., 2020), and in unbinned contigs from
215 marine hydrate-bearing sediments from offshore Shimokita Peninsula (Kawai et al., 2014 mbsf,
216 core S12H4;). AtiR was also found in *Firmicutes* from other depths in Site 1244, including
217 *Clostridia* MAG 1244-F3-H4-B2, *Firmicutes* MAG 1244-F2-H4-B10, and *Aminicenantes* MAG
218 1244-C3H4-B23. AtiR was also found in *Omnitrophica* genomes from Mid-Cayman Rise vent
219 fluid plumes and in JS-1 genomes from Aarhus Bay, Denmark. Genes downstream of *atiR* were
220 dominated by transporters for organic solutes (*tct, dct, ugp*), branched chain amino acids (*liv*),
221 hydrolases (choline sulfatase, sialidase, tryptophanase, cysteine desulfurase), peptidases,
222 racemases, and RTX-toxin (Tables S6; Fig. 5A). XRE regulators are widely distributed across the
223 tree of life and regulate diverse metabolic functions and oxidative stress responses, typically as
224 repressors that bind to DNA (Fig. 5B) to prevent transcription in the absence of a ligand. Methane-
225 hydrate bacteria may use AtiR to regulate cellular degradation of peptides and proteins to amino
226 acids, either for nutrient acquisition or for survival under environmental stress (Bergkessel et al.,
227 2016).

228 **Osmotic stress survival.** Any life that can persist in brine pockets within methane hydrate
229 must contend with high salinity (up to ~3x that of seawater) and low water potential. We found a
230 K^+ stimulated pyrophosphatase, which is involved in salt stress in other bacteria (López-Marqués

231 et al., 2004; Tsai et al., 2014), expressed the GHSZ sample (Table 1). *Atribacteria* MAG E10H5-
232 B2 also contained numerous genes for the "salt out" survival strategy, in which osmotic pressure
233 is maintained by exporting cations (Wood, 2015). Cation export systems included efflux systems,
234 mechanosensitive ion channels, and Na^+-H^+ antiporters (Table 2). *Atribacteria* MAG E10H5-B2
235 also contained numerous MazEF toxin-antitoxin systems (Table S7), which are involved in
236 translational control during stress response (Culviner and Laub, 2018).

237 A second salt survival strategy is import and/or biosynthesis of osmolytes, most often polar,
238 water-soluble, and uncharged organic compounds and/or extracellular polymers. For example,
239 glycine betaine is abundant in saline fluids from deep sediment basins (Daly et al., 2016).
240 *Atribacteria* MAG E10H5-B2 contained genes for transport of trehalose and biosynthesis of the
241 common osmolytes glutamine, glutamate, and poly-gamma-glutamate, all of which had homologs
242 in other *Atribacteria* MAGs (Table 2). A capsular polysaccharide biosynthesis protein was among
243 the handful of confident peptide hits (Table 1). *Atribacteria* transcripts for trehalose synthesis and
244 transport were also present in other marine sediments (Bird et al., 2019). *Atribacteria* MAG E10H5-
245 B2 also contained multiple copies of the aromatic amino acid exporter *yddG*, one of the most highly
246 transcribed *Atribacteria* genes in other marine sediments (Bird et al., 2019). B2 and another
247 *Atribacteria* MAG from a marine mud volcano (UBA9904) encoded myo-inositol-1 phosphate
248 synthase (MIPS)/bifunctional IPC transferase and DIPP synthase (IPCT-DIPPS) for the unusual
249 solute di-myo-inositol-phosphate (DIP; Table 2), which was previously only known to be made by
250 hyperthermophiles (Santos and Da Costa, 2002).

251 The capacity for glycosylation may be another adaptation for survival of salt stress (Kho
252 and Meredith, 2018). *Atribacteria* MAG E10H5-B2 and other *Atribacteria* encoded the non-
253 mevalonate pathway for isoprenoid biosynthesis (*ispDEFGH*), exopolysaccharide synthesis
254 proteins, numerous glycosyltransferases for transferring UDP- and GDP-linked sugars to a variety
255 of substrates, and several proteins related to N-linked glycosylation (Table S8). Carbohydrate
256 active enzymes are secreted by *Atribacteria* (Orsi et al., 2018) and may be involved in stress

response. *Atribacteria* MAG E10H5-B2 also encoded genes for propionate catabolism and a bacterial microcompartment superlocus with 94-99% amino acid identity to a *Atribacteria* SAG from the Marianas Trench (Fig. S2), which is thought to be involved in sugar and aldehyde metabolism in *Atribacteria* (Axen et al., 2014; Nobu et al., 2016).

Adaptations to life in methane hydrates. Microbes in the GHSZ in deep subsurface sediments appear to contain unique adaptations for survival in an extreme system with high salinity, high pressure, and low temperatures. Other probable environmental stress adaptations may include glycosylation and membrane modifications. It is also possible that these microbes can produce secondary metabolites that modify gas hydrate properties; we recently showed experimentally that recombinant *Chloroflexi* proteins from metagenomic sequences native to methane hydrate-bearing sediments alter the structure of clathrates (Johnson et al., 2020). More experiments are required to resolve the complex metabolic pathways and biosynthetic potential of life in methane hydrates, with important implications for stability of gas hydrates on our own planet (e.g. Snyder et al., 2020) and potential habitability and survival strategies of other planetary bodies in our solar system (Mousis et al., 2015; Kamata et al., 2019).

Acknowledgments. We thank Vinayak Agarwal, Brett Baker, Jennifer Biddle, Jordan Bird, Anirban Chakraborty, Frederick Colwell, Sheng Dai, Xiyang Dong, Konstantinos Konstantinidis, Peter Girguis, Julie Huber, Casey Hubert, Raquel Lieberman, Karen Lloyd, Katie Marshall, Alejandra Prieto Davo, Brandi Reese, Claudia Remes, Emil Ruff, Anne Trehu, Despina Tsementzi, Paula Welander, Loren Williams, Jieying Wu, and Jenny Yang for helpful discussions; Phil Rumford and curatorial staff at the ODP Gulf Coast Repository for providing samples; and Shweta Biliya, Annie Hartwell, Janet Hatt, Mike Lee, Nastassia Patin, Ben Tully, and the Bioinformatics Virtual Coordination Network for technical assistance with sequencing and bioinformatic analysis. This research was funded by Center for Dark Energy Biosphere Investigations (C-DEBI) Small Research Grant to J.B.G. and C.B.K. (NSF OCE-0939564), NASA Exobiology grant to J.B.G. and

F.J.S. (NNX14AJ87G), NSF Biology Oceanography grant to F.J.S and J.B.G. (NSF OCE-1558916), NASA Exobiology grant to J.B.G. (80NSSC19K0477), and a Georgia Tech Earth and Atmospheric Sciences Frontiers Postdoctoral Fellowship to C.B.K. Metaproteomic analysis by B.L.N. was partially supported by the University of Washington's Proteomic Resource (UWPR95794). This is C-DEBI contribution [provided upon paper acceptance].

Experimental Procedures

Sample collection. Sediments were cored at ODP site 1244 (44°35.1784´N; 125°7.1902´W; 895 m water depth; **Fig. S1**) on the eastern flank of Hydrate Ridge ~3 km northeast of the southern summit on ODP Leg 204 in 2002 (Tréhu et al., 2003) and stored at -80°C at the ODP Gulf Coast Repository.

Geochemistry. Data for dissolved methane, sulfate, manganese, iron, and iodide in sediment porewaters were obtained from Tréhu et al. (2003). Reactive iron and manganese were extracted from frozen sediments using the citrate-dithionite method (Roy et al., 2013) and measured by inductively coupled plasma optical emission spectrometer (Agilent Technologies 700 Series). Total carbon, total nitrogen and total sulfur were determined by CNS analyzer (Perkin Elmer 2400). Total inorganic carbon was measured by CO_2 coulometer (CM5130) with a CM5130 acidification module. Geochemical metadata are given in Table S1 and archived in BCO-DMO project 626690.

DNA extraction. DNA was extracted, in duplicate, from 8-20 g of sediment from the following depths in meters below seafloor (mbsf, using IODP core designations, see (ShipboardScientificParty, 2003)): 1.95-2.25 (C1-H2); 3.45-3.75 (C1-H3); 8.60 (F2-H4); 18.10 (F3-H4); 20.69 (C3-H4); 35.65 (E5-H5); 68.55 (E10-H5); 138.89 (core E19-H5) using a MO-BIO PowerSoil total RNA Isolation Kit with the DNA Elution Accessory Kit, following the manufacturer protocol without beads. DNA pellets from two replicates from each depth were pooled together. DNA concentrations were measured using a Qubit 2.0 fluorometer with dsDNA High Sensitivity reagents (Invitrogen, Grand Island, NY, USA). DNA yields ranged from 4-15 ng per gram of sediments. Core E19-H5 (139 mbsf) yielded only 2 ng DNA per gram of sediment and yielded unreliable data due to contamination with sequences from the enzymes used in the library preparations. Therefore, this core segment was excluded from further analysis.

16S rRNA gene amplicon sequencing. Microbial community composition was assessed by Illumina sequencing of the V3-V4 region of the 16S rRNA gene. The V3-V4 region was PCR-amplified using primers F515 and R806 (Caporaso et al., 2011), each appended with barcodes and Illumina-specific adapters according to (Kozich et al., 2013). Reactions consisted of 1-2 µL DNA template (2 ng), 5 µL of 10x Taq Mutant reaction buffer, 0.4 µL of Klentaq LA Taq Polymerase (DNA Polymerase Technology, St. Louis, MO, USA), 2 µL of 10 mM dNTP mix (Sigma Aldrich, St. Louis, MO, USA), 2 µL of reverse and forward primers (total concentration 0.4 µM), and DNA-free water (Ambion, Grand Island, NY, USA) for the remainder of the 50 µL total volume. PCR conditions were an initial 5-min denaturation at 94°C, followed by 35 cycles of denaturation at 94°C (40 sec), primer annealing at 55°C (40 sec), and primer extension at 68°C (30 sec). Amplicon libraries were purified using a QIAquick PCR Purification Kit (Qiagen, Germantown, MD, USA), quantified by Qubit (Life Technologies), and pooled in equimolar concentration. Amplicons were sequenced on an Illumina MiSeq across two runs using the V2 500-cycle kit with 5% PhiX to increase read diversity. 16S rRNA sequences were deposited into NCBI SAMN04214977-04214990 (PRJNA295201).

16S rRNA gene amplicon taxonomic analysis. 16S rRNA sequences were trimmed using Trim Galore (criteria: length >100 bp length, Phred score >25). Sequences were dereplicated with a cutoff of 200 bp, chimeras were removed, and ASVs were resolved using deblur (Amir et al., 2017). Shannon and chao 1 diversity indices were calculated in R using phyloseq (McMurdie and Holmes, 2013).

***Atribacteria* ASV phylogenetic analysis.** The reference alignment included *Atribacteria* 16S rRNA gene sequences from environmental clones from Inagaki et al. (2006); Nobu et al. (2016),

339 Carr et al. (2015), and Yarza et al. (2014). The alignment was trimmed to include only the V3-V4
340 region spanned by the *Atribacteria* ASV sequences, resulting in a final alignment with 198 bases.
341 The DNA sequences were aligned in MAFFT with the L-INS-i option (Katoh and Standley, 2013).
342 A neighbor-joining phylogeny with 100 bootstraps was rooted with members of the *Synergistetes*
343 bacterial phylum.
344
345 **Multiple displacement amplification, library preparation, and sequencing**. Genomic DNA was
346 amplified from all samples using a REPLI-g Single Cell Kit (Qiagen, Germantown, MD, USA)
347 using UV-treated sterile plasticware and reverse transcription-PCR grade water (Ambion, Grand
348 Island, NY, USA). Quantitative PCR showed that the negative control began amplifying after 5 hr
349 of incubation at 30°C, and therefore, the 30°C incubation step was shortened to 5 hr using a Bio-
350 Rad C1000 Touch thermal cycler (Bio-Rad, Hercules, CA, USA). DNA concentrations were
351 measured by Qubit. Two micrograms of MDA-amplified DNA were used to generate genome
352 libraries using a TruSeq DNA PCR-Free Kit following the manufacturer's protocol (Illumina, San
353 Diego, CA, USA). The resulting libraries were sequenced using a Rapid-Run on an Illumina HiSeq
354 2500 to obtain 100 bp paired-end reads. Sequencing statistics are provided in Table S3.
355
356 **Metagenome assembly, binning, and annotation.** Demultiplexed Illumina reads were mapped to
357 known adapters using Bowtie2 in local mode to remove any reads with adapter contamination.
358 Demultiplexed Illumina read pairs were quality trimmed with Trim Galore (Babraham
359 Bioinformatics) using a base Phred33 score threshold of Q25 and a minimum length cutoff of 80
360 bp. Paired-end reads were then assembled into contigs using SPAdes assembler with --meta option
361 for assembling metagenomes, iterating over a range of k-mer values
362 (21,27,33,37,43,47,51,55,61,65,71,75,81,85,91,95). Assemblies were assessed with reports
363 generated with QUAST. Features on contigs were predicted through the Prokka pipeline with
364 Barrnap for rRNA, Aragorn for tRNA, Infernal and Rfam for other non-coding RNA, and Prodigal
365 for protein coding genes. Metagenomic 16S rRNA sequences predicted by Barrnap were analyzed
366 by BLASTN analysis against the SILVA SSU database version 138.
367 Annotation of protein-coding genes was performed as follows: 1) BLASTP search against
368 the default set of core genomes, followed by HMM search against a set of default core HMM
369 profiles available in Prokka, 2) use of the BLAST Descriptor Annotator algorithm in BLAST2GO,
370 which conducts BLAST against the NCBI nr database, 3) KEGG orthology assignment using
371 GhostKoala and 4) InterProScan analysis, which involves cross-reference HMM searches across
372 multiple databases to find Pfam families with close homology. Metagenomic sequences were
373 deposited into NCBI SAMN07256342-07256348 (PRJNA390944). Whole Genome Shotgun
374 projects has been deposited at DDBJ/ENA/GenBank under the accession JABUBK000000000-
375 JABUBQ000000000.
376
377 **Metagenome-assembled genomes.** Metagenome contigs were partitioned through MetaBAT
378 (Kang et al., 2015) into metagenome-assembled genomes (MAGs) using tetranucleotide frequency
379 and sequencing depth. Sequencing depth was estimated by mapping reads on to assembled contigs
380 using Bowtie2 and Samtools. Completeness, contamination and strain level heterogeneity were
381 assessed using single copy marker genes in CheckM (Parks et al., 2015). Gene features and their
382 functional annotations for genome bins were extracted from the metagenome for the contigs that
383 belong to the bins. Taxonomic affiliation for each bin was inferred via the least common ancestor
384 (LCA) algorithm in MEGAN6 and by the top BLAST matches to the marker gene *rpoB*. Twenty-
385 one MAGs with estimated completeness >50% were deposited into GenBank (Table S3). The B2
386 MAG was deposited into GenBank as "Candidatus *Atribacteria* bacterium 1244-E10-H5-B2"
387 (SAMN07342547; NMQN00000000.1). Read recruitments of metagenomic sequences to MAGs
388 were performed using Bowtie2 (Langmead and Salzberg, 2012) normalized to the approximate
389 number of genomes in the metagenome estimated with MicrobeCensus (Nayfach and Pollard,

390 2015). The average amino acid identity matrix was generated using the ANI-AAI matrix tool
391 (Rodriguez-R and Konstantinidis, 2016).
392
393 ***Atribacteria* MAG and SAG phylogeny.** Public *Atribacteria* single cell amplified genomes
394 (SAGs) or MAGs (77 genomes, as of July 2020) were collected into a Genome Group workspace
395 in Pathosystems Resource Integration Center (PATRIC; Wattam et al., 2014). Six ribosomal
396 proteins from the large rRNA subunit (L2, L3, L4, L6, L16, L18) and two from the large rRNA
397 subunit (S3 and S19) were collected from the *Atribacteria* genomes using the Features tab in
398 Genome Group View. The eight ribosomal proteins were concatenated and the amino acid
399 sequences were aligned in MAFFT with the L-INS-i option (Katoh and Standley, 2013). A
400 neighbor-joining phylogeny with 1000 bootstraps was rooted with members of the *Synergistetes*
401 bacterial phylum.
402
403 **Maximum likelihood phylogenies.** Large subunit hydrogenase (HunG) and the xenobiotic
404 response element regulator (AtiR) were made using sequences aligned in MAFFT with the L-INS-
405 i option (Katoh and Standley, 2013). Neighbor-joining phylogenies were made with 100 bootstraps.
406
407 **Gene neighborhood diagrams.** Gene neighborhood diagrams for the *hun* gene neighborhood were
408 made using the gene neighborhood tool (GNT) in EFI web tools using a "single sequence BLAST"
409 function in "Retrieve Neighborhood Diagrams" set to an E-value of 10^{-5} and a window size of 20
410 (Zallot et al., 2019). The input sequence was NCBI accession RXG63129 for HunG.
411
412 **Metaproteomic sample preparation, mass spectrometry, and data analyses.** Proteins from
413 E10-H5 were extracted from a 10 g of frozen sediment using a protocol adapted from Nicora et al.
414 (2013). Briefly, 2.5 mL of desorption buffer (0.5 M NaCl, 0.1 M glycerol, 0.2% SDS, 6 M urea, 1
415 mM EDTA, 100 mM ammonium bicarbonate) and 2 mL of a pH-buffered amino acid solution
416 (containing equimolar histidine, lysine, and arginine, all 83 g 1 L-1 in ultra-pure water, pH 7.0)
417 was added to the sample on ice. The goal of the pH-buffered amino acid solution is to fill the
418 electronegative mineral sites in the sample with positively charged amino acids to reduce
419 absorption of proteins to the particles. Samples were vortexed 4x, alternating 5 minutes vortexing
420 and 5 min ice. The sediment slurry was then sonicated with Bronson probe sonicator (4 x 30 s) to
421 lyse cells and heated at 95°C for 5 min. The sediment was pelleted by centrifugation (10,000 x g,
422 30 min, 4°C), and the supernatant was collected and stored on ice. The sediment pellet was washed
423 2 more times with 3 mL desorption buffer and supernatants were combined. In order to remove the
424 SDS prior to protein digestion and mass spectrometry analysis, the filter aided sample preparation
425 (FASP) method was used (Ostasiewicz et al., 2010). Millipore Amicon 10 kDa filter units were
426 used and cleaned following manufacturer's directions. Samples were loaded on top of filters (~9
427 mL) and centrifuged (3000 rpm, 90 min, 4°C). To remove all SDS, proteins retained on the filter
428 were rinsed 3 times by adding 5 mL of 8 M urea in 50 mM ammonium bicarbonate and repeating
429 the prior centrifugation step. Iodoacetamide (3 mL, 15 mM) was added to samples, incubated in
430 the dark at room temperature for 30 minutes, and then centrifuged (3000 rpm, 90 min, 4°C).
431 Proteins were then rinsed two times with 10 mL of 100 mM ammonium bicarbonate and centrifuged
432 to remove liquid (3000 rpm, 90 min, 4°C). To digest protein on the filter, 0.5 µg of trypsin
433 (modified, sequencing grade, Promega) was added to the filter, topped with 2.5 mL of 25 mM
434 ammonium bicarbonate, vortexed, and incubated 12 hr at room temperature. Filtrate was collected
435 by centrifugation (3000 rpm, 90 min, 4°C), and SpeedVaced to near dryness at 4oC. Peptides were
436 then resuspended in 50 µL of 2% acetonitrile and 0.1% formic acid and desalted using Nest Group
437 C18 Proto centrifugal macro columns following manufacturer's instructions. Each 10 µL sample
438 was separated on a NanoAquity UPLC with a 60 min gradient (2-35% acetonitrile) and analyzed
439 on a Thermo Scientific Orbitrap Fusion Tribrid Mass Spectrometer operated in top20 data
440 dependent acquisition mode.

441 A protein database for identifying the collected fragmentation spectra was generated from
442 *Atribacteria* MAGs (C1H2_C3H4ab_E10H5_contam.fasta). These databases were concatenated
443 with 50 common contaminants, yielding a protein database of 10,325 proteins. To assign spectra to
444 peptide sequences, correlative database searches were completed using Comet v. 2015.01 rev. 2
445 (Eng et al., 2013; Eng et al., 2015). Comet parameters included: trypsin enzyme specificity, semi-
446 digested, allowance of 1 missed cleavage, 10 ppm mass tolerance, cysteine modification of 57 Da
447 (resulting from the iodoacetamide) and modifications on methionine of 15.999 Da (oxidation).
448 Minimum protein and peptide thresholds were set at $P > 0.95$ on Protein and Peptide Prophet
449 (Nesvizhskii et al., 2003). Protein inferences from the whole-cell lysates were accepted by
450 ProteinProphet if the thresholds noted above were passed, two or more peptides were identified,
451 and at least one terminus was tryptic (Keller et al., 2002; Nesvizhskii et al., 2003; Pedrioli, 2010).
452 For each peptide discussed in the manuscript, manual inspection of the spectral identification was
453 completed. The mass spectrometry proteomics data have been deposited to the ProteomeXchange
454 Consortium via the PRIDE partner repository (Vizcaíno et al., 2015) with the dataset
455 identifier PXD012479 (https://www.ebi.ac.uk/pride/archive/ Login: reviewer08969@ebi.ac.uk
456 Password: BP2V3yGA).

457 **Table 1.** Peptide hits for ODP Site 1244 sample E10-H5 (~69 mbsf). Matches are shown
458 for >70% identity to non-Hydrate Ridge genomes.
459

Peptide	NCBI accession number	Conserved domains	Top hit, NCBI accession (% identity)
EYKPKEDWKMNFSSSY NLNTK	RXG64736	LPS-assembly protein LptD	OQY39007 (82%), *Atribacteria* 4572_76, Guaymas Basin, Gulf of California
YSLKQMVLPILIGLIAPIII GFTLGVWPLAAFLIGVK IVGALLA	MBA7568979	K^+-stimulated pyrophosphate-energized proton pump HppA	HDP36765 (91%), *Atribacteria* SpSt-1160, contaminated groundwater, New York, USA
PRMLSYILLALSLSLILL KFFK	MQY74719	Tripartite tricarboxylate transporter TctB	N/A
PVSAAINLIHLLPIPLLIQ RDLKEK	RXG64647	Tripartite ATP-independent periplasmic transporter DctQ	N/A
NKINLIFSILIIIFLIVLTYE GIILVKVGLNA	RXG62936	Tripartite ATP-independent periplasmic transporter DctQ	N/A
CSNLIIKALLVVLVLSLG ITLGIAKAP	RXG64193	Basic membrane lipoprotein BmpA	PKP58720 (94%), *Atribacteria* HGW-1, groundwater, Horonobe URL, Japan
KPFRKSPGLIILLSTVAV GFIIR	MBA7587931	High-affinity branched-chain amino acid transport system permease protein LivH	TET08159 (99%), *Atribacteria* E44_bin65, Gulf of Mexico petroleum seepage sediments
GIIILIFLIAVITAVLVSYF VLSPTP	RXG64813	Capsular polysaccharide biosynthesis protein	HBY56740 (76%), *Atribacteria* UBA9904, petroleum reservoir, North Slope Alaska

460

461 **Table 2. Putative osmotic stress-related genes in *Atribacteria* MAG E10-H5 B2.**
462 *indicates multiple copies.

Annotation	**Gene**	**Accession**	**Top hit (% identity)**	***Atribacteria* MAG with top hit**	**Top hit environment and reference for metagenomes**
Na^+ efflux	*natB*	RXG65900	TET06401 (98%)	E44_bin65	Gulf of Mexico petroleum seep sediments (Chakraborty et al., 2020)
Na^+ channel	DUF554	RXG63559	TET10447 (99%)		
K^+ transport	*trkAH**	RXG63511 RXG63512	TET06940 (97%) TET06939 (99%)		
Mechanosensitive ion channel	*mscS*	RXG63036	TET10003 (97%)		
Glutamine synthetase	*glnA*	RXG65164	TET08352 (99%)		
Trehalose transporter	*sugAB*	RXG66833-RXG66834	KUK55397- (94%) KUK55398 (99%)	34_128	Oil reservoir, North Slope, Alaska (Hu et al., 2016)
Threonine/lysine efflux	*rhtB*	RXG66248	KUK55393 (91%)		
Na^+/H^+ antiporter	*mrpEFGB*	RXG65834-RXG65838	TFB09297-TFB09301 (91-95%)	MT.SAG.1	Marianas Trench (Peoples et al., 2019)
Aromatic amino acid exporter	*yddG**	RXG63201	TFB08968 (91%)		
Glutamate synthase	*gltD*	RXG66270	PKP56573 (94%)	HGW-1	Horonobe Underground Laboratory, Japan (Hernsdorf et al., 2017)
Proline racemase	*prdF*	RXG63210	PKP58887 (92%)		
Poly-gamma glutamate synthase	*pgsCBW*	RXG66317-RXG66319	PKP60458-PKP60460 (~90%)		
DIPP synthesis pathway	MIPS/IPCT-DIPPS*	RXG66889-RXG66888	HBY57541-HBY57542 (~80%)	UBA9904	Haakon Mosby mud volcano, Barents Sea (Niemann et al., 2006)

463

464

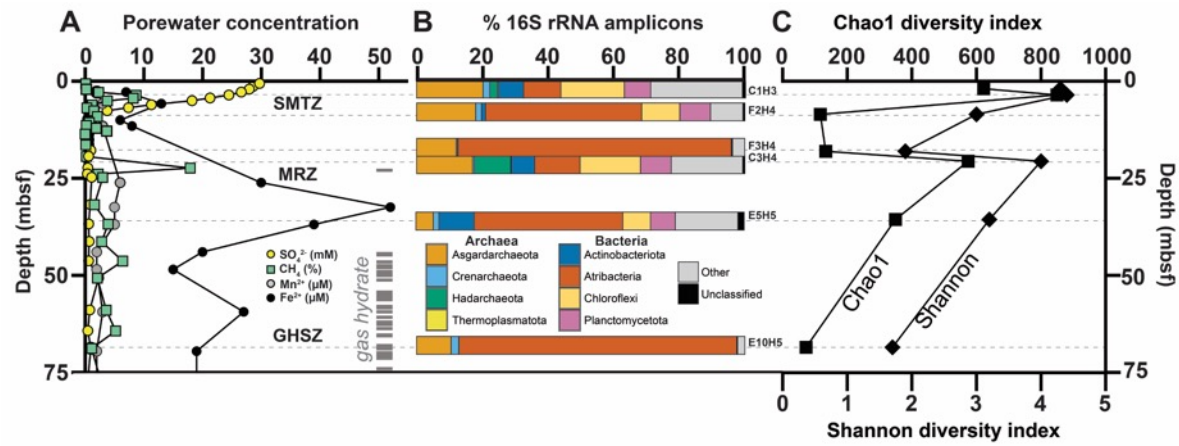

Figure 1: Porewater geochemistry and microbial taxonomy and diversity from sediment depth profiles at ODP 204 Site 1244, Hydrate Ridge, offshore Oregon, USA. **A:** Sulfate (yellow circles), methane (green squares), manganese (gray circles), and iron (black circles) concentrations, and depth of gas hydrate occurrences (gray dashes) from Tréhu et al. (2003). Sulfate and methane data are from core 1244B. Iron and manganese data are from core 1244E. Gas hydrate occurrence data are from core 1244C and 1244E. SMTZ: sulfate-methane transition zone; MRZ: metal reduction zone; GHSZ: gas hydrate stability zone. **B:** 16S rRNA gene amplicon taxonomic composition at the phylum level. "Other" category represents bacterial and archaeal phyla with <10% of total sequences. "Unclassified" represents sequences that were not classified at the phylum level. 16S rRNA amplicon data not shown for core C1H2 (see text). **C:** Microbial diversity based on Chao1 (top axis, squares) and Shannon index (bottom axis, diamonds) for the same 16S rRNA gene amplicon samples as shown in panel B.

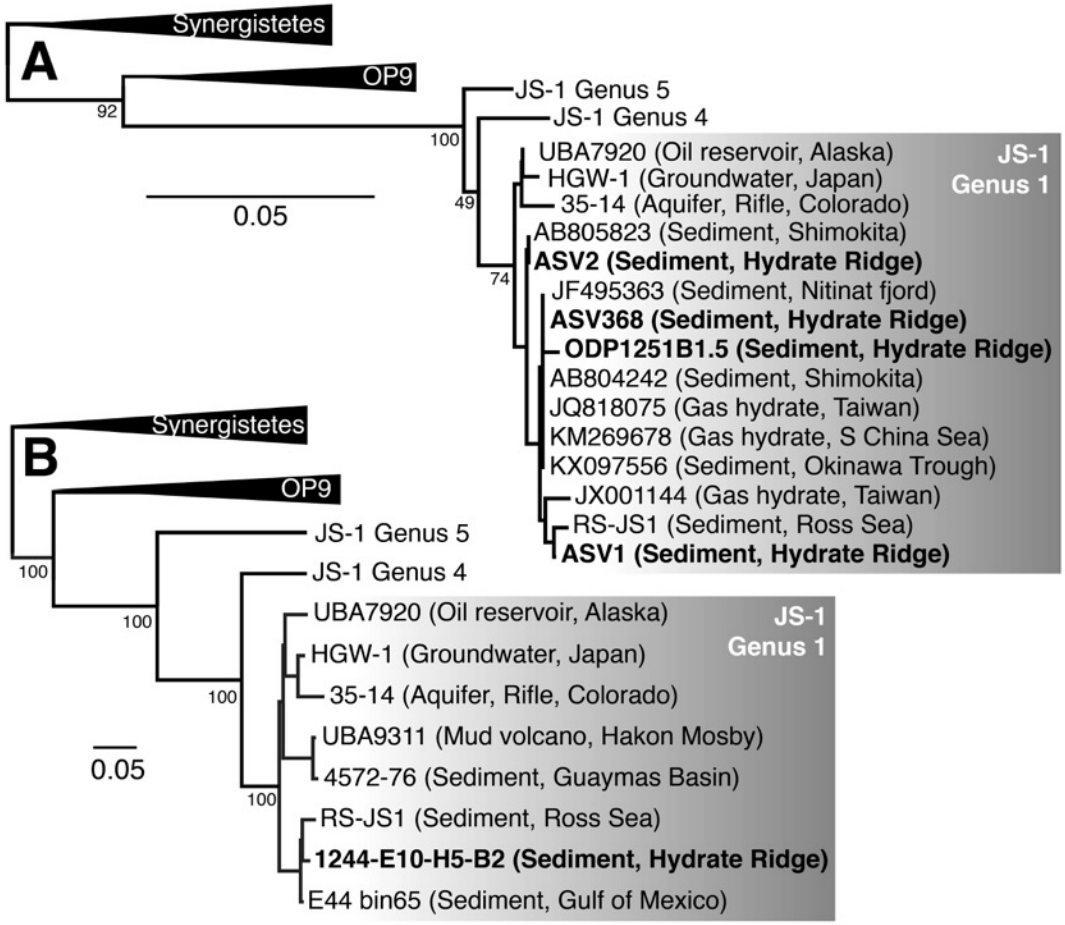

Figure 2: Neighbor-joining *Atribacteria* JS-1 Genus 1 phylogenies based on (A) 16S rRNA amplicons and (B) ribosomal proteins. Bolded sequences are from Hydrate Ridge. 16S rRNA phylogeny including the top three most abundant Atribacteria ASVs from Site 1244 (see Table S2 for relative sequence abundances). ODP1251B1.5 is the dominant JS-1 16S rRNA clone from Hydrate Ridge Leg 204 cores as reported by Inagaki et al. (2006). Italicized names are from MAGs or SAGs; the rest of the sequences are from 16S amplicons. Genera labels are based on sequences from Yarza et al. (2014) and Liu et al. (2019). Conserved sites used in phylogenies: (A) 190 bases; (B) 846 amino acids.

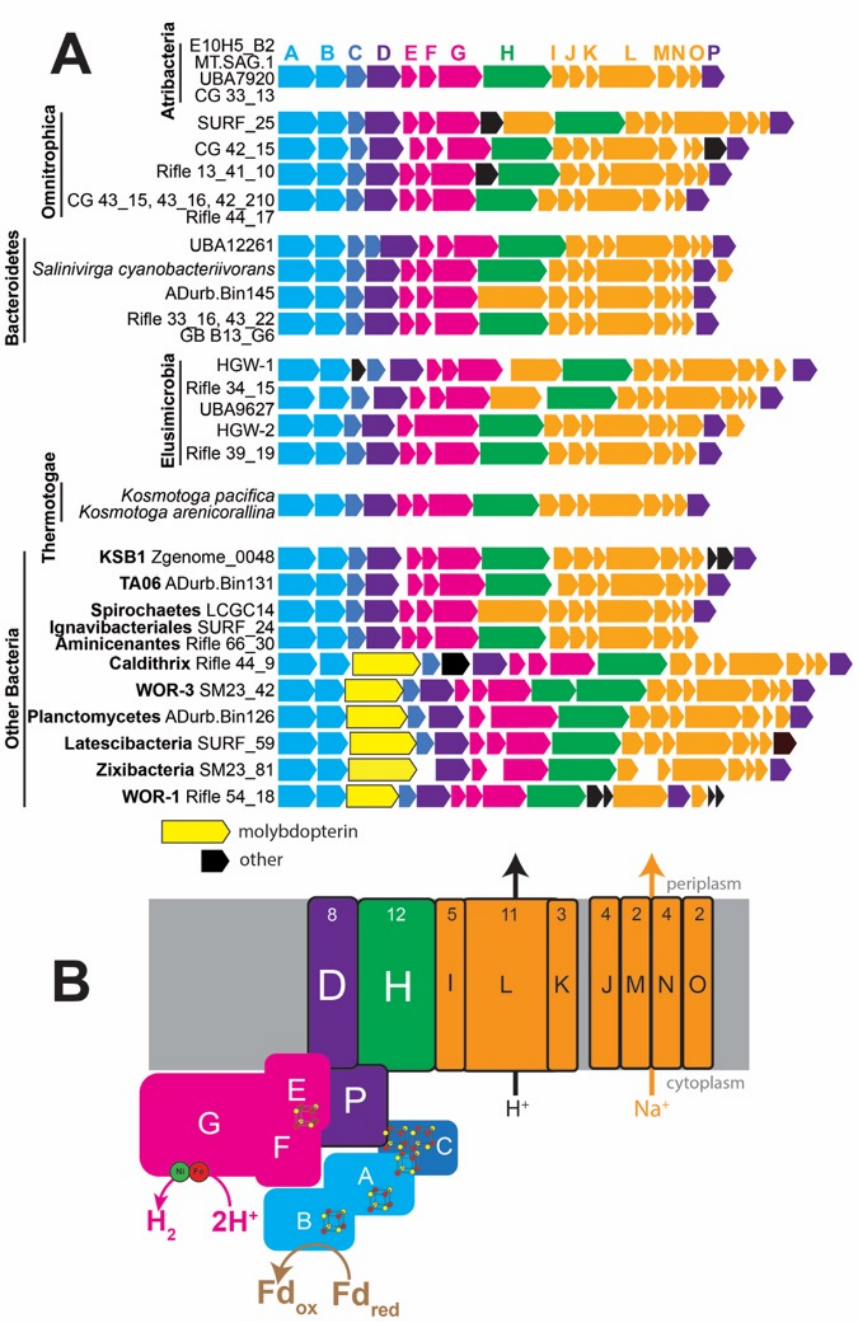

Figure 3: Gene neighborhood and predicted function of the predicted multi-subunit Hun respiratory complex. A: conserved gene cluster arrangement, with each color representing a different predicted protein. Some gene arrangements are found in more than one genome, as indicated. All MAGs and SAGs are from sediment samples. Sample abbreviations: ADurb: wastewater; CG: Crystal Geyser, Utah, USA; GB: Guaymas Basin, Gulf of California; HGW: Horonobe Underground Laboratory, Japan; LCGC: Loki's Castle, Mid-Atlantic Ridge, Atlantic Ocean; MT: Mariana Trench; SM: White Oak Estuary, North Carolina, USA; SURF: Stanford Underground Research Facility, South Dakota, USA; Rifle: Rifle research site, Colorado, USA; UBA12261: wetland surface sediment; UBA9627: Rifle research site, Colorado, USA. **B:** predicted cellular locations and functions based on homologs of the genes of the same colors encoded by the putative *hun* operon in panel A. Iron-sulfur clusters and the Ni-Fe active site of HunG are also shown.

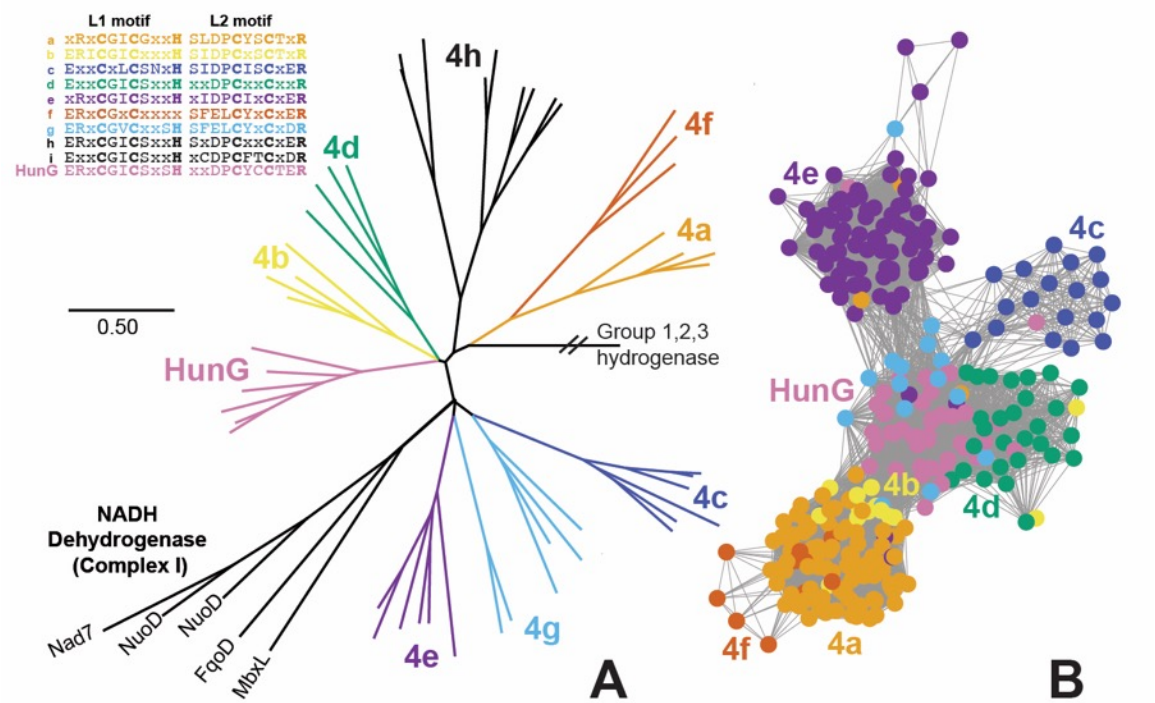

Figure 4: Phylogeny and sequence clustering of HunG and related large-subunit hydrogenases from group 4. A: Maximum likelihood HunG/NuoD/HycE phylogeny, with [Ni-Fe] hydrogenase group 4 labels drawn based on naming system from Søndergaard et al. (2016) and L1 and L2 motifs for the large subunit metal-binding centers for each class of group 4 hydrogenase. The NuoD subunit of NADH dehydrogenase (Complex I), which evolved from group 4 hydrogenase (Schut et al., 2016), is also included. **B:** Sequence similarity network for Group 4a,b,c,d,e,f,g and HunG hydrogenases with E-value cutoff of 10^{-90} and group color scheme the same as in A. Subgroups 4h and 4i are not shown in the sequence similarity network because they had no edges to the larger Group 4 cluster at E-value cutoff of 10^{-90}.

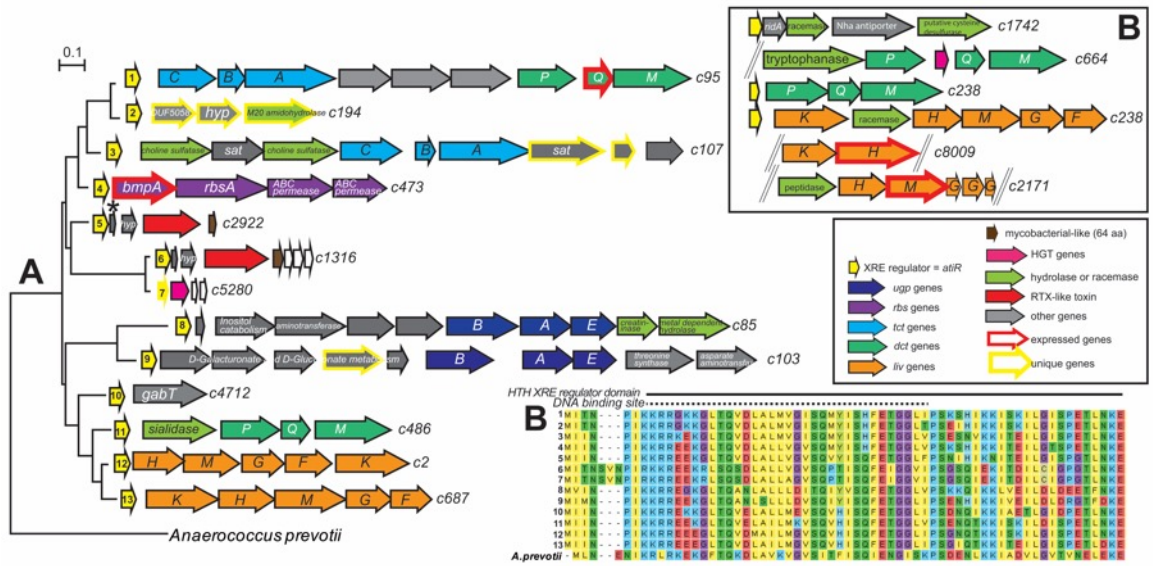

Figure 5: Phylogeny of helix-turn-helix xenobiotic response element regulators (yellow), hereafter "AtiR", from B2 and synteny of downstream genes. Genes highlighted in thick red lines were expressed in the metaproteome. **A:** AtiR maximum likelihood phylogeny based on contigs (labeled on the right) from E10-H5 B2, with *Anaerococcus prevotii* as the outgroup. **Top inset:** Additional putative operons from B2 likely regulated by *atiR*, which is truncated partially or completely on these contigs. **Bottom inset:** Legend for panels A and B; **B:** AtiR amino acid alignment for the N-terminus of 13 AtiR sequences from *Atribacteria* E10-H5-B2 shown in panel A. Abbreviations: *bmpA*: basic membrane protein A; *dctPQM*: C4-dicarboxylate transporter; *gabT*: 4-aminobutyrate aminotransferase; *livHMGF*: branched chain amino acid transporter; *rbs*: ribose transporter; *sat:* sulfate adenylyltransferase; *tctCBA*: tricarboxylate transporter; *ugpBAE*: sn-glycerol-3-phosphate transporter. See Table S6 for accession numbers and % identity to closest gene hits in other genomes.

526 **References**

527 Amir, A., McDonald, D., Navas-Molina, J.A., Kopylova, E., Morton, J.T., Xu, Z.Z. et al.
528 (2017) Deblur rapidly resolves single-nucleotide community sequence patterns. *MSystems*
529 **2**.

530 Archer, D., Buffett, B., and Brovkin, V. (2009) Ocean methane hydrates as a slow tipping
531 point in the global carbon cycle. *Proc Natl Acad Sci* **106**: 20596-20601.

532 Aromokeye, D.A., Oni, O.E., Tebben, J., Yin, X., Richter-Heitmann, T., Wendt, J. et al.
533 (2020) Crystalline iron oxides stimulate methanogenic benzoate degradation in marine
534 sediment-derived enrichment cultures. *The ISME Journal* **15**: 1-16.

535 Axen, S.D., Erbilgin, O., and Kerfeld, C.A. (2014) A taxonomy of bacterial
536 microcompartment loci constructed by a novel scoring method. *PLoS Comput Biol* **10**:
537 e1003898.

538 Bergkessel, M., Basta, D.W., and Newman, D.K. (2016) The physiology of growth arrest:
539 uniting molecular and environmental microbiology. *Nature Reviews Microbiology* **14**: 549.

540 Bird, J.T., Tague, E.D., Zinke, L., Schmidt, J.M., Steen, A.D., Reese, B. et al. (2019)
541 Uncultured microbial phyla suggest mechanisms for multi-thousand-year subsistence in
542 Baltic Sea sediments. *Mbio* **10**: e02376-02318.

543 Blazejak, A., and Schippers, A. (2010) High abundance of JS-1-and Chloroflexi-related
544 Bacteria in deeply buried marine sediments revealed by quantitative, real-time PCR. *FEMS*
545 *Microbiology Ecology* **72**: 198-207.

546 Bohrmann, G., and Torres, M.E. (2006) Gas Hydrates in Marine Sediments. In *Marine*
547 *Geochemistry*. Schulz, H.D., and Zabel, M. (eds). Berlin, Heidelberg: Springer, pp. 481-
548 512.

549 Caporaso, J.G., Lauber, C.L., Walters, W.A., Berg-Lyons, D., Lozupone, C.A., Turnbaugh,
550 P.J. et al. (2011) Global patterns of 16S rRNA diversity at a depth of millions of sequences
551 per sample. *Proc Natl Acad Sci* **108**: 4516-4522.

552 Carr, S.A., Orcutt, B.N., Mandernack, K.W., and Spear, J.R. (2015) Abundant Atribacteria
553 in deep marine sediment from the Adelie Basin, Antarctica. *Front Microbiol* **6**: 872.

554 Chakraborty, A., Ruff, S., Dong, X., Ellefson, E., Li, C., Brooks, J. et al. (2020)
555 Hydrocarbon seepage in the deep seabed links subsurface and seafloor biospheres. *Proc*
556 *Natl Acad Sci* **117**: 11029-11037.

557 Chernitsyna, S., Mamaeva, E., Lomakina, A., Pogodaeva, T., Galach'yants, Y.P., Bukin,
558 S. et al. (2016) Phylogenetic diversity of microbial communities of the Posolsk Bank
559 bottom sediments, Lake Baikal. *Microbiology* **85**: 672-680.

560 Collett, T., Bahk, J.-J., Baker, R., Boswell, R., Divins, D., Frye, M. et al. (2015) Methane
561 Hydrates in Nature □ Current Knowledge and Challenges. *Journal of chemical &*
562 *engineering data* **60**: 319-329.

563 Culviner, P.H., and Laub, M.T. (2018) Global analysis of the E. coli toxin MazF reveals
564 widespread cleavage of mRNA and the inhibition of rRNA maturation and ribosome
565 biogenesis. *Molecular cell* **70**: 868-880. e810.

566 Daly, R.A., Borton, M.A., Wilkins, M.J., Hoyt, D.W., Kountz, D.J., Wolfe, R.A. et al.
567 (2016) Microbial metabolisms in a 2.5-km-deep ecosystem created by hydraulic fracturing
568 in shales. *Nat Microbiol* **1**: 16146.

569 Dodsworth, J.A., Blainey, P.C., Murugapiran, S.K., Swingley, W.D., Ross, C.A., Tringe,
570 S.G. et al. (2013) Single-cell and metagenomic analyses indicate a fermentative and
571 saccharolytic lifestyle for members of the OP9 lineage. *Nat Commun* **4**: 1854.

572 Dong, X., Greening, C., Rattray, J.E., Chakraborty, A., Chuvochina, M., Mayumi, D. et al.
573 (2019) Metabolic potential of uncultured bacteria and archaea associated with petroleum
574 seepage in deep-sea sediments. *Nature communications* **10**: 1-12.

575 Eng, J.K., Jahan, T.A., and Hoopmann, M.R. (2013) Comet: an open‐source MS/MS
576 sequence database search tool. *Proteomics* **13**: 22-24.

577 Eng, J.K., Hoopmann, M.R., Jahan, T.A., Egertson, J.D., Noble, W.S., and MacCoss, M.J.
578 (2015) A deeper look into Comet—implementation and features. *J Am Soc Mass Spec* **26**:
579 1865-1874.

580 Fischer, M., Hopkins, A.P., Severi, E., Hawkhead, J., Bawdon, D., Watts, A.G. et al. (2015)
581 Tripartite ATP-independent periplasmic (TRAP) transporters use an arginine-mediated
582 selectivity filter for high affinity substrate binding. *J Biol Chem* **290**: 27113-27123.

583 Fry, J.C., Parkes, R.J., Cragg, B.A., Weightman, A.J., and Webster, G. (2008) Prokaryotic
584 biodiversity and activity in the deep subseafloor biosphere. *FEMS Microbiol Ecol* **66**: 181-
585 196.

586 Gies, E.A., Konwar, K.M., Beatty, J.T., and Hallam, S.J. (2014) Illuminating microbial
587 dark matter in meromictic Sakinaw Lake. *Appl Environ Microbiol* **80**: 6807-6818.

588 Greening, C., Biswas, A., Carere, C.R., Jackson, C.J., Taylor, M.C., Stott, M.B. et al.
589 (2016) Genomic and metagenomic surveys of hydrogenase distribution indicate H 2 is a
590 widely utilised energy source for microbial growth and survival. *The ISME journal* **10**:
591 761-777.

592 Gründger, F., Carrier, V., Svenning, M.M., Panieri, G., Vonnahme, T.R., Klasek, S., and
593 Niemann, H. (2019) Methane-fuelled biofilms predominantly composed of methanotrophic
594 ANME-1 in Arctic gas hydrate-related sediments. *Scientific reports* **9**: 1-10.

Hernsdorf, A.W., Amano, Y., Miyakawa, K., Ise, K., Suzuki, Y., Anantharaman, K. et al. (2017) Potential for microbial H2 and metal transformations associated with novel bacteria and archaea in deep terrestrial subsurface sediments. *ISME J* **11**: 1915-1929.

Hester, K.C., and Brewer, P.G. (2009) Clathrate hydrates in nature. *Ann Rev Mar Sci* **1**: 303-327.

Honkalas, V., Dabir, A., and Dhakephalkar, P.K. (2016) Life in the Anoxic Sub-Seafloor Environment: Linking Microbial Metabolism and Mega Reserves of Methane Hydrate. In *Anaerobes in Biotechnology*. Hatti-Kaul, R., Mamo, G., and Mattiasson, B. (eds). Cham: Springer, pp. 235-262.

Hoshino, T., Toki, T., Ijiri, A., Morono, Y., Machiyama, H., Ashi, J. et al. (2017) Atribacteria from the subseafloor sedimentary biosphere disperse to the hydrosphere through submarine mud volcanoes. *Front Microbiol* **8**: 1135.

Hoshino, T., Doi, H., Uramoto, G.-I., Wörmer, L., Adhikari, R.R., Xiao, N. et al. (2020) Global diversity of microbial communities in marine sediment. *Proceedings of the National Academy of Sciences*.

Hu, P., Tom, L., Singh, A., Thomas, B.C., Baker, B.J., Piceno, Y.M. et al. (2016) Genome-resolved metagenomic analysis reveals roles for candidate phyla and other microbial community members in biogeochemical transformations in oil reservoirs. *mBio* **7**: e01669-01615.

Inagaki, F., Suzuki, M., Takai, K., Oida, H., Sakamoto, T., Aoki, K. et al. (2003) Microbial communities associated with geological horizons in coastal subseafloor sediments from the Sea of Okhotsk. *Appl Environ Microbiol* **69**: 7224-7235.

Inagaki, F., Nunoura, T., Nakagawa, T., Teske, A., Lever, M.A., Lauer, A. et al. (2006) Biogeographical distribution and diversity of microbes in methane hydrate-bearing deep marine sediments on the Pacific Ocean Margin. *Proc Natl Acad Sci* **103**: 2815–2820.

Johnson, A.M., Huard, D.J., Kim, J., Raut, P., Dai, S., Lieberman, R.L., and Glass, J.B. (2020) Mainly on the Plane: Deep Subsurface Bacterial Proteins Bind and Alter Clathrate Structure. *Crystal Growth & Design*.

Kadnikov, V.V., Mardanov, A.V., Beletsky, A.V., Shubenkova, O.V., Pogodaeva, T.V., Zemskaya, T.I. et al. (2012) Microbial community structure in methane hydrate-bearing sediments of freshwater Lake Baikal. *FEMS Microbiol Ecol* **79**: 348-358.

Kamata, S., Nimmo, F., Sekine, Y., Kuramoto, K., Noguchi, N., Kimura, J., and Tani, A. (2019) Pluto's ocean is capped and insulated by gas hydrates. *Nature Geoscience* **12**: 407-410.

Kang, D.D., Froula, J., Egan, R., and Wang, Z. (2015) MetaBAT, an efficient tool for accurately reconstructing single genomes from complex microbial communities. *PeerJ* **3**: e1165.

632 Kastner, M., Kvenvolden, K.A., and Lorenson, T.D. (1998) Chemistry, isotopic
633 composition, and origin of a methane-hydrogen sulfide hydrate at the Cascadia subduction
634 zone. *Earth and Planetary Science Letters* **156**: 173-183.

635 Katayama, T., Nobu, M.K., Kusada, H., Meng, X.-Y., Yoshioka, H., Kamagata, Y., and
636 Tamaki, H. (2020) Isolation of a member of the candidate phylum 'Atribacteria' reveals a
637 unique cell membrane structure. *Nature Communications* **11**: 6381.

638 Katoh, K., and Standley, D.M. (2013) MAFFT multiple sequence alignment software
639 version 7: improvements in performance and usability. *Molecular biology and evolution*
640 **30**: 772-780.

641 Kawai, M., Futagami, T., Toyoda, A., Takaki, Y., Nishi, S., Hori, S. et al. (2014) High
642 frequency of phylogenetically diverse reductive dehalogenase-homologous genes in deep
643 subseafloor sedimentary metagenomes. *Frontiers in microbiology* **5**: 80.

644 Keller, A., Purvine, S., Nesvizhskii, A.I., Stolyar, S., Goodlett, D.R., and Kolker, E. (2002)
645 Experimental protein mixture for validating tandem mass spectral analysis. *OMICS* **6**: 207-
646 212.

647 Kho, K., and Meredith, T.C. (2018) Salt-induced stress stimulates a lipoteichoic acid-
648 specific three component glycosylation system in *Staphylococcus aureus*. *J Bacteriol* **200**:
649 e00017-00018.

650 Kormas, K.A., Smith, D.C., Edgcomb, V., and Teske, A. (2003) Molecular analysis of deep
651 subsurface microbial communities in Nankai Trough sediments (ODP Leg 190, Site 1176).
652 *FEMS Microbiol Ecol* **45**: 115-125.

653 Kozich, J.J., Westcott, S.L., Baxter, N.T., Highlander, S.K., and Schloss, P.D. (2013)
654 Development of a dual-index sequencing strategy and curation pipeline for analyzing
655 amplicon sequence data on the MiSeq Illumina sequencing platform. *Appl Environ*
656 *Microbiol* **79**: 5112-5120.

657 Kvenvolden, K.A. (1993) A primer on gas hydrates. *US Geological Survey professional*
658 *paper* **1570**: 279-291.

659 Langmead, B., and Salzberg, S.L. (2012) Fast gapped-read alignment with Bowtie 2.
660 *Nature methods* **9**: 357.

661 Lanoil, B.D., Sassen, R., La Duc, M.T., Sweet, S.T., and Nealson, K.H. (2001) Bacteria
662 and Archaea physically associated with Gulf of Mexico gas hydrates. *Appl Environ*
663 *Microbiol* **67**: 5143-5153.

664 Lee, Y.M., Hwang, K., Lee, J.I., Kim, M., Hwang, C.Y., Noh, H.-J. et al. (2018) Genomic
665 insight into the predominance of candidate phylum *Atribacteria* JS1 lineage in marine
666 sediments. *Front Microbiol* **9**: 2909.

667 Li, T., and Wang, P. (2013) Biogeographical distribution and diversity of bacterial
668 communities in surface sediments of the South China Sea. *J Microbiol Biotechnol* **23**: 602-
669 613.

670 Lin, L.-H., Wu, L.-W., Cheng, T.-W., Tu, W.-X., Lin, J.-R., Yang, T.F. et al. (2014)
671 Distributions and assemblages of microbial communities along a sediment core retrieved
672 from a potential hydrate-bearing region offshore southwestern Taiwan. *J Asian Earth Sci*
673 **92**: 276-292.

674 Liu, Y.-F., Qi, Z.-Z., Shou, L.-B., Liu, J.-F., Yang, S.-Z., Gu, J.-D., and Mu, B.-Z. (2019)
675 Anaerobic hydrocarbon degradation in candidate phylum 'Atribacteria' (JS1) inferred from
676 genomics. *The ISME Journal* **13**: 2377-2390.

677 López-Marqués, R.L., Pérez-Castiñeira, J.R., Losada, M., and Serrano, A. (2004)
678 Differential regulation of soluble and membrane-bound inorganic pyrophosphatases in the
679 photosynthetic bacterium Rhodospirillum rubrum provides insights into pyrophosphate-
680 based stress bioenergetics. *Journal of bacteriology* **186**: 5418-5426.

681 Mazurenko, L., and Soloviev, V. (2003) Worldwide distribution of deep-water fluid
682 venting and potential occurrences of gas hydrate accumulations. *Geo-Marine Letters* **23**:
683 162-176.

684 McMurdie, P.J., and Holmes, S. (2013) phyloseq: an R package for reproducible interactive
685 analysis and graphics of microbiome census data. *PloS one* **8**: e61217.

686 Milkov, A.V., Dickens, G.R., Claypool, G.E., Lee, Y.-J., Borowski, W.S., Torres, M.E. et
687 al. (2004) Co-existence of gas hydrate, free gas, and brine within the regional gas hydrate
688 stability zone at Hydrate Ridge (Oregon margin): evidence from prolonged degassing of a
689 pressurized core. *Earth Planet Sci Lett* **222**: 829-843.

690 Mousis, O., Chassefiere, E., Holm, N.G., Bouquet, A., Waite, J.H., Geppert, W.D. et al.
691 (2015) Methane clathrates in the solar system. *Astrobiology* **15**: 308-326.

692 Nayfach, S., and Pollard, K.S. (2015) Average genome size estimation improves
693 comparative metagenomics and sheds light on the functional ecology of the human
694 microbiome. *Genome Biology* **16**: 51.

695 Nesvizhskii, A.I., Keller, A., Kolker, E., and Aebersold, R. (2003) A statistical model for
696 identifying proteins by tandem mass spectrometry. *Anal Chem* **75**: 4646-4658.

697 Newberry, C.J., Webster, G., Cragg, B.A., Parkes, R.J., Weightman, A.J., and Fry, J.C.
698 (2004) Diversity of prokaryotes and methanogenesis in deep subsurface sediments from
699 the Nankai Trough, Ocean Drilling Program Leg 190. *Environ Microbiol* **6**: 274-287.

700 Nicora, C.D., Anderson, B.J., Callister, S.J., Norbeck, A.D., Purvine, S.O., Jansson, J.K.
701 et al. (2013) Amino acid treatment enhances protein recovery from sediment and soils for
702 metaproteomic studies. *Proteomics* **13**: 2776-2785.

703 Niemann, H., Lösekann, T., De Beer, D., Elvert, M., Nadalig, T., Knittel, K. et al. (2006)
704 Novel microbial communities of the Haakon Mosby mud volcano and their role as a
705 methane sink. *Nature* **443**: 854-858.

706 Nobu, M.K., Narihiro, T., Rinke, C., Kamagata, Y., Tringe, S.G., Woyke, T., and Liu, W.-
707 T. (2015) Microbial dark matter ecogenomics reveals complex synergistic networks in a
708 methanogenic bioreactor. *ISME J* **9**: 1710-1722.

709 Nobu, M.K., Dodsworth, J.A., Murugapiran, S.K., Rinke, C., Gies, E.A., Webster, G. et al.
710 (2016) Phylogeny and physiology of candidate phylum 'Atribacteria' (OP9/JS1) inferred
711 from cultivation-independent genomics. *ISME J* **10**: 273-286.

712 Orsi, W.D., Richards, T.A., and Francis, W.R. (2018) Predicted microbial secretomes and
713 their target substrates in marine sediment. *Nature microbiology* **3**: 32-37.

714 Ostasiewicz, P., Zielinska, D.F., Mann, M., and Wiśniewski, J.R. (2010) Proteome,
715 phosphoproteome, and N-glycoproteome are quantitatively preserved in formalin-fixed
716 paraffin-embedded tissue and analyzable by high-resolution mass spectrometry. *J Prot Res*
717 **9**: 3688-3700.

718 Parkes, R.J., Cragg, B., Roussel, E., Webster, G., Weightman, A., and Sass, H. (2014) A
719 review of prokaryotic populations and processes in sub-seafloor sediments, including
720 biosphere: geosphere interactions. *Mar Geol* **352**: 409-425.

721 Parks, D.H., Imelfort, M., Skennerton, C.T., Hugenholtz, P., and Tyson, G.W. (2015)
722 CheckM: assessing the quality of microbial genomes recovered from isolates, single cells,
723 and metagenomes. *Genome Res* **25**: 1043-1055.

724 Pedrioli, P.G. (2010) Trans-Proteomic Pipeline: A Pipeline for Proteomic Analysis. In
725 *Proteome Bioinformatics*. Hubbard, S., and Jones, A. (eds): Humana Press, pp. 213-238.

726 Peoples, L.M., Grammatopoulou, E., Pombrol, M., Xu, X., Osuntokun, O., Blanton, J. et
727 al. (2019) Microbial community diversity within sediments from two geographically
728 separated hadal trenches. *Frontiers in microbiology* **10**: 347.

729 Reed, D.W., Fujita, Y., Delwiche, M.E., Blackwelder, D.B., Sheridan, P.P., Uchida, T.,
730 and Colwell, F.S. (2002) Microbial communities from methane hydrate-bearing deep
731 marine sediments in a forearc basin. *Appl Environ Microbiol* **68**: 3759-3770.

732 Rinke, C., Schwientek, P., Sczyrba, A., Ivanova, N.N., Anderson, I.J., Cheng, J.-F. et al.
733 (2013) Insights into the phylogeny and coding potential of microbial dark matter. *Nature*
734 **499**: 431-437.

735 Rodriguez-R, L.M., and Konstantinidis, K.T. (2016) The enveomics collection: a toolbox
736 for specialized analyses of microbial genomes and metagenomes. In: PeerJ Preprints.

737 Rosa, L.T., Bianconi, M.E., Thomas, G.H., and Kelly, D.J. (2018) Tripartite ATP-
738 independent periplasmic (TRAP) transporters and tripartite tricarboxylate transporters

(TTT): from uptake to pathogenicity. *Frontiers in cellular and infection microbiology* **8**: 33.

Roy, M., McManus, J., Goni, M.A., Chase, Z., Borgeld, J.C., Wheatcroft, R.A. et al. (2013) Reactive iron and manganese distributions in seabed sediments near small mountainous rivers off Oregon and California (USA). *Cont Shelf Res* **54**: 67-79.

Ruff, S., Felden, J., Gruber-Vodicka, H., Marcon, Y., Knittel, K., Ramette, A., and Boetius, A. (2019) In situ development of a methanotrophic microbiome in deep-sea sediments. *The ISME journal* **13**: 197.

Ruppel, C.D., and Kessler, J.D. (2017) The interaction of climate change and methane hydrates. *Rev Geophys* **55**: 126-168.

Santos, H., and Da Costa, M.S. (2002) Compatible solutes of organisms that live in hot saline environments. *Environ Microbiol* **4**: 501-509.

Schut, G.J., Zadvornyy, O., Wu, C.-H., Peters, J.W., Boyd, E.S., and Adams, M.W. (2016) The role of geochemistry and energetics in the evolution of modern respiratory complexes from a proton-reducing ancestor. *Biochimica et Biophysica Acta (BBA)-Bioenergetics* **1857**: 958-970.

ShipboardScientificParty (2003) Site 1244. In *Proc ODP, Init Repts, 204*. Tréhu, A., Bohrmann, G., Rack, F., Torres, M., and al., e. (eds). College Station, TX: Ocean Drilling Program, pp. 1–132 doi:110.2973/odp.proc.ir.2204.2103.2003.

Snyder, G.T., Matsumoto, R., Suzuki, Y., Kouduka, M., Kakizaki, Y., Zhang, N. et al. (2020) Evidence in the Japan Sea of microdolomite mineralization within gas hydrate microbiomes. *Scientific reports* **10**: 1-13.

Søndergaard, D., Pedersen, C.N., and Greening, C. (2016) HydDB: a web tool for hydrogenase classification and analysis. *Scientific reports* **6**: 1-8.

Tréhu, A., Bohrmann, G., Rack, F., and Torres, M. (2003) Volume 204 Initial Reports. In *Proc ODP, Initial Reports*, pp. 77845-79547.

Tréhu, A.M., Long, P.E., Torres, M.E., Bohrmann, G., Rack, F.R., Collett, T.S. et al. (2004) Three-dimensional distribution of gas hydrate beneath southern Hydrate Ridge: constraints from ODP Leg 204. *Earth and Planetary Science Letters* **222**: 845-862.

Tsai, J.-Y., Kellosalo, J., Sun, Y.-J., and Goldman, A. (2014) Proton/sodium pumping pyrophosphatases: the last of the primary ion pumps. *Current opinion in structural biology* **27**: 38-47.

Ussler III, W., and Paull, C.K. (2001) Ion exclusion associated with marine gas hydrate deposits. In *Natural Gas Hydrates: Occurrence, Distribution, and Detection*. Paull, C.K., and Dillion, W.P. (eds): American Geophysical Union.

Vetting, M.W., Al-Obaidi, N., Zhao, S., San Francisco, B., Kim, J., Wichelecki, D.J. et al. (2015) Experimental strategies for functional annotation and metabolism discovery: targeted screening of solute binding proteins and unbiased panning of metabolomes. *Biochemistry* **54**: 909-931.

Vizcaíno, J.A., Csordas, A., Del-Toro, N., Dianes, J.A., Griss, J., Lavidas, I. et al. (2015) 2016 update of the PRIDE database and its related tools. *Nuc Acid Res* **44**: D447-D456.

Vuillemin, A., Vargas, S., Coskun, Ö.K., Pockalny, R., Murray, R.W., Smith, D.C. et al. (2020) Atribacteria reproducing over millions of years in the Atlantic abyssal subseafloor. *mBio* **11**.

Wattam, A.R., Abraham, D., Dalay, O., Disz, T.L., Driscoll, T., Gabbard, J.L. et al. (2014) PATRIC, the bacterial bioinformatics database and analysis resource. *Nucleic acids research* **42**: D581-D591.

Webster, G., Parkes, R.J., Fry, J.C., and Weightman, A.J. (2004) Widespread occurrence of a novel division of bacteria identified by 16S rRNA gene sequences originally found in deep marine sediments. *Appl Environ Microbiol* **70**: 5708-5713.

Webster, G., Yarram, L., Freese, E., Koster, J., Sass, H., Parkes, R.J., and Weightman, A.J. (2007) Distribution of candidate division JS1 and other Bacteria in tidal sediments of the German Wadden Sea using targeted 16S rRNA gene PCR-DGGE. *FEMS Microbiol Ecol* **62**: 78-89.

Whiticar, M.J., Hovland, M., Kastner, M., and Sample, J.C. (1995) 26. ORGANIC GEOCHEMISTRY OF GASES, FLUIDS, AND HYDRATES AT THE CASCADIA ACCRETIONARY MARGIN. In *Proceedings of the Ocean Drilling Program, Scientific Results*.

Wood, J.M. (2015) Bacterial responses to osmotic challenges. *J Gen Physiol* **145**: 381-388.

Yanagawa, K., Kouduka, M., Nakamura, Y., Hachikubo, A., Tomaru, H., and Suzuki, Y. (2014) Distinct microbial communities thriving in gas hydrate-associated sediments from the eastern Japan Sea. *Journal of Asian Earth Sciences* **90**: 243-249.

Yarza, P., Yilmaz, P., Pruesse, E., Glöckner, F.O., Ludwig, W., Schleifer, K.-H. et al. (2014) Uniting the classification of cultured and uncultured bacteria and archaea using 16S rRNA gene sequences. *Nat Rev Microbiol* **12**: 635-645.

Zallot, R., Oberg, N., and Gerlt, J.A. (2019) The EFI web resource for genomic enzymology tools: leveraging protein, genome, and metagenome databases to discover novel enzymes and metabolic pathways. *Biochemistry* **58**: 4169-4182.

Zhou, Z., Liu, Y., Xu, W., Pan, J., Luo, Z.-H., and Li, M. (2020) Genome-and community-level interaction insights into carbon utilization and element cycling functions of Hydrothermarchaeota in hydrothermal sediment. *Msystems* **5**.